RSC Advances




ROYAL SOCIETY OF CHEMISTRY

www.rsc.org/advances

Journal Name

RSCPublishing

PAPER

# Mineral carbonation of desulfurization residue for $CO_2$ sequestration

Cite this: DOI: 10.1039/x0xx00000x

Wenjin Ding [a,b], and Huaming Yang [a,b,c,*], Jing Ouyang [a,b,*]

Received 00th January 2012,
Accepted 00th January 2012

DOI: 10.1039/x0xx00000x

www.rsc.org/

The feasibility of mineral carbonation of desulfurization residue for sequestering $CO_2$ was evaluated both through theoretical and experimental approaches. The carbonation reaction, including carbonation of $Ca(OH)_2$ and $CaSO_4$, occurred through a kinetically controlled stage with an activation energy of 20.21 kJ $mol^{-1}$. Concentration of ammonia, $CO_2$ flow rate, liquid to solid ratio and temperature impacted on the carbonation ratio of desulfurization residue through their direct and definite influence on the rate constant. Concentration of ammonia and liquid to solid ratio were the most important factors influencing the desulfurization residue carbonation in terms of both the carbonation ratio and reaction rate. Under optimized conditions the carbonation ratio could reach approximately 98% when using industry-grade $CO_2$. The crystalline phase of the carbonated desulfurization residue was calcite and vaterite with spherical and granular morphology. The $CO_2/O_2/N_2$ mixed gas was also used as the simulated desulfurization fuel gas in the carbonation reaction and it had a relatively minor effect on the carbonation ratio. However, it slowed the carbonation reaction and produced a carbonation product with a smaller average particle size, which included high purity (≥99%) white calcite. The desulfurization residue carbonation reported herein showed a rapid $CO_2$ sequestration ratio, high $CO_2$ sequestration amounts, low costs, and a large potential for in-situ $CO_2$ sequestration in the electricity and steel industry.

## 1. Introduction

Current warming of the global climate is considered to be caused by increasing emissions of anthropogenic greenhouse gases since pre-industrial times, in particular the emissions of $CO_2$[1-3]. The control of greenhouse gas emissions is arguably the most challenging environmental policy issue that has been encountered, both in China and elsewhere[4-6]. Continued uncontrolled greenhouse gas emissions may lead to rising sea levels and species extinction. In 2013, global $CO_2$ emissions hit a new record, reaching about 36.1 billion tons. Among them, China's emissions of 10 billion tons, accounting for nearly a third of the global $CO_2$ emissions[7]. The global carbon cycle is sufficiently extensive to conclude that natural processes cannot absorb all the anthropogenically produced carbon dioxide ($CO_2$) in the coming centuries, so adaptation technologies are urgently required[8, 9]. Mineral carbonation has recently been considered as a leading method for $CO_2$ sequestration. The technology is based on the reaction of $CO_2$ with an alkaline metal oxide to form stable carbonates, typically of calcium ($CaCO_3$) or magnesium ($MgCO_3$). Many natural minerals containing large quantities of primary cations ($Ca^{2+}$ and $Mg^{2+}$), such as olivine, serpentine and wollastonite, have been evaluated for $CO_2$ sequestration[9-17]. The carbonation of natural minerals often requires harsh reaction conditions because the natural minerals are thermodynamically stable. Furthermore, the added costs of mining, grinding, and separation of natural minerals from the source rock, which is in some sense also a waste of resources, make natural mineral carbonation less applicable to industrial development[18].

Solid wastes may also contain many alkaline metal ions, and their use for $CO_2$ sequestration has several advantages over using natural minerals. The advantages offered by solid wastes include: (1) they supply a readily available source of calcium or magnesium mineral matter without any need for pre-processing; (2) they are typically fine-grained with high reactive surface areas; (3) the environmental quality of the waste materials accumulation area can be improved through pH-neutralization and mineral transformation; and (4) the carbonation product may be amenable for beneficial reuse as road base or other construction materials[19, 20]. Researchers have studied carbonation with a range of wastes including steel slag[21-24], mining residues[25], coal ash[26], and waste concrete and blast furnace slag[27, 28]. Desulfurization residue is a kind of solid wastes, and it is mostly generated during the process of removing $SO_x$ from flue gas streams from power generation and sintering plants. The residue generally contains rich calcium. And desulfurization residue

[a] *Centre for Mineral Materials, School of Minerals Processing and Bioengineering, Central South University, Changsha 410083, China*

[b] *Key Laboratory for Mineral Materials and Application of Hunan Province, Central South University, Changsha 410083, China*

[c] *State Key Laboratory of Powder Metallurgy, Central South University, Changsha 410083, China*

**Corresponding author, email: hmyang@csu.edu.cn, jingouyang@csu.edu.cn. Tel.: +86-731-88830549, Fax: +86-731-88710804.*

is produced in the form of a fine powder, it can be used directly in the carbonation process without pre-processing. Approximately 20 Mt of desulfurization residue is produced in China each year with only 15% of this being recycled[29], suggesting that approximately 5-7 Mt of $CO_2$ could be sequestered annually if all available desulfurization residue were used for mineral carbonation.

To our knowledge, there have few reports about the flue gas desulfurization gypsum carbonation for $CO_2$ sequestration[30-32], but they all focused on the effects of process conditions on the results, and the composition of desulfurization gypsum is much simpler than that of desulfurization residue.

In this paper, desulfurization residue was used in the carbonation experiments, and ammonia was employed as the reaction media to speed up the reaction. The feasibility of this route was investigated by using both theoretical and experimental approaches. The underlying mechanism was further discussed by kinetic analysis during the carbonation reaction.

## 2. Experimental

### 2.1 Materials preparation

The desulfurization residue, with clubbed and granular morphology (Fig. 1a&b), used in this study was obtained from China Wuhan Iron and Steel Corp. The main phase of the desulfurization residue sample was gypsum that also contained some calcium hydroxide (Fig. 1c). The major constituents were CaO, $SO_3$ and combined water, and the major impurities were $SiO_2$, $Fe_2O_3$ and $Al_2O_3$. The detailed composition is presented in Table 1. The particle size was measured using a particle size analyzer (LS-POP(6), Zhuhai OMEC Instrument Co., Ltd., China). The average ($d_{50}$) particle size was 35.92 μm and over 90% of the particles were smaller than 80 μm (Fig. 1d). Gaseous $CO_2$ was first supplied from bottled sources at industry-grade of 99.9% purity. In later tests $CO_2$ was supplied as a part of a mixture that simulated desulfurized flue gas. After removal of $SO_x$, desulfurized flue gas typically contains 5%–10% $CO_2$, 10%–15% $O_2$, 75%–80% $N_2$. To evaluate the feasibility of the carbonation experiment with a $CO_2/O_2/N_2$ gas mixture similar to that from a steel or iron plant a mixture of 75% $N_2$, 15% $O_2$ and 10% $CO_2$ was used.

For each experiment 20 g of desulfurization residue was placed into a 400-mL reaction vessel with a predetermined volume and concentration of ammonia solution then added. A magnetic stirrer was used to ensure adequate mixing while a hot-water bath maintained the desired reaction temperature. The $CO_2$-rich gas was injected with a predetermined flow rate at normal pressure. A pH meter was installed to monitor the progress of the carbonation reaction. The pH value was recorded at 2-min intervals until the pH value was relatively constant. The mixture was then filtered to separate the solids from the solution before the solids were washed with distilled water and dried in an oven at 110°C for approximately 24 h. Detailed experimental conditions for each set of experiments are listed in Table 2.

### 2.2 Characterization

The composition of the sample was determined by X-ray fluorescence (XRF) and chemical titration. Powder XRD measurements of the samples were conducted with a DX-2700 X-ray diffractometer using Cu Kα radiation (λ = 0.15406 nm) at a scanning ratio of 0.02 deg/s with a voltage of 40 kV at 40 mA. SEM was performed by a JEOL JSM-6360LV scanning electron microanalyzer with an accelerating voltage of 5 kV. The carbonation ratio ($\eta$) and the $CO_2$ sequestration efficiency (ε) were calculated according to the following equation:

$$\eta = \frac{\frac{MW_{Ca}}{MW_{CaCO_3}} \times C_2 \times M_2}{C_1 \times M_1} \times 100\% \quad (1)$$

$$\varepsilon = \frac{C_2 \times M_2 \times \frac{MW_{CO_2}}{MW_{CaCO_3}}}{v \times C_3 \times t \times \rho} \times 100\% \quad (2)$$

where $M_1$ is the mass of desulfurization residue, $C_1$ is the percentage of calcium in desulfurization residue, $M_2$ is the mass of carbonation products and $C_2$ is the percentage of calcium carbonate in the carbonation products. $M_1$ and $M_2$ were obtained by direct weighing. The calcium content was measured by a process involving a number of stages. First a 250 g/L NaCl solution was reacted with $CaSO_4 \cdot 2H_2O$ with 10% acetic acid then reacted with any $Ca(OH)_2$ to liberate $Ca^{2+}$ ions. The total $Ca^{2+}$ content of the desulfurization residue filtrate ($C_1$) was then determined using the EDTA titration method. The Ca-phases in the carbonation products were predominantly $CaCO_3$ and $CaSO_4$, with only the former reacting with 0.5% acetic acid. This allowed the percentage of calcium carbonate in the carbonation products ($C_2$) to be calculated. Carbonation was only assumed to occur to calcium because the contributions from other metals (e.g. Mg, Fe) were considered to be small in comparison. v is the $CO_2$ (or simulated flue gas) flow rate, t is the injecting time, ρ is the density of $CO_2$ (or simulated flue gas) and $C_3$ is the purity of the injecting $CO_2$ (or simulated flue gas). v, t, ρ and $C_3$ are known.

## 3. Results and discussion

In the gas-liquid-solid system, the overall possible chemical reactions are expressed by Eqs. (3)-(6). To illustrate the theoretical feasibility of the route proposed above, the thermodynamic parameters at the standard state in the carbonation processes of desulfurization residue were calculated.

$$Ca(OH)_2(aq)+CO_2(aq)\rightarrow CaCO_3(s) + H_2O(l) \quad (3)$$
$$\Delta G(kJ/mol)= -75 \qquad K=1.40\times10^{13}$$

$$2NH_4OH(aq)+CO_2(aq)\rightarrow (NH_4)_2CO_3(aq)+H_2O(l) \quad (4)$$
$$\Delta G(kJ/mol)= -276 \qquad K=2.40\times10^{48}$$

$$CaSO_4(s)+(NH_4)_2CO_3(aq)\rightarrow CaCO_3(s)+(NH_4)_2SO_4(aq) \quad (5)$$
$$\Delta G(kJ/mol)= -22 \qquad K=7.18\times10^{3}$$

$$Ca(OH)_2(aq)+(NH_4)_2CO_3(aq)\rightarrow CaCO_3(s)+2NH_4OH(aq) \quad (6)$$
$$\Delta G(kJ/mol)= +201 \qquad K= -1.71\times10^{35}$$

From the thermodynamic calculation results, the gibbs free energy changes ($\Delta G$) are -75, -276 and -22 kJ/mol for Eqs. (3)-(5). They are all less than zero. And their corresponding equilibrium constants (K) are $1.40\times10^{13}$, $2.40\times10^{48}$ and $7.18\times10^{3}$. They are all

greater than zero. So, Eqs. (3)-(5) can proceed spontaneously, and they can be regarded as the irreversible exothermic reaction. The gibbs free energy change ($\Delta G$) is +201 kJ/mol $>0$ for equation (6). And the corresponding equilibrium constant (K) is $-1.71\times10^{35}<0$. So, equation (6) can not proceed spontaneously in the carbonation process. Through the above analysis, the proposed route is theoretically feasible. And the desulfurization residue carbonation can be summarized into the following two steps: carbonation of $Ca(OH)_2$ and carbonation of $CaSO_4$.

The influence of concentration of ammonia, $CO_2$ flow rate, liquid to solid ratio and temperature on the carbonation of desulfurization residue were shown in Fig.s 2-5, respectively. Fig. 2a showed the change of the pH of the reaction solution with time. The initial pH value was approximately 12.5 but decreased over time as the ammonia reacted to form ammonium carbonate, while the carbonation ratio gradually increased (Fig. 2b). Values of pH eventually stabilized at approximately 7, which signified the end of the reaction. Except for A1 (1 mol/L) and A2 (2 mol/L), the carbonation ratios were over 90% when the carbonation reactions were finished. In the cases of both A1 and A2, however, the carbonation reaction was not completed due to a lack of ammonia. Because the carbonation ratio did not increase after 60 min, then it should correspond to the virtual termination of the reaction, which was confirmed from pH value of 7. Thus, it could be determined that the termination time of carbonation was simply by monitoring the pH variation time as shown in Fig. 2a. For the high ammonia experiment, A4 (4 mol/L), the high terminal pH value of 7.6 indicated that there was excess ammonia, thus 3 mol/L was chosen as the optimum ammonia concentration.

The effect of the $CO_2$ flow rate on the desulfurization residue carbonation was evaluated by considering $CO_2$ flow rates of 50, 100 and 200 mL/min (B1, B2 and A3, respectively). At 200 mL/min, the pH of the solution reached 7, indicating that the reaction had completed, after 50 min (Fig. 3a). When the flow rate was decreased to 100 and 50 mL/min, the time required for the pH to reach 7 increased to 55 and 80 min, respectively. This suggested that an increase in the $CO_2$ flow rate accelerated the carbonation reaction. In addition, Fig. 3b showed that over 90% of the gypsum and calcium hydroxide were converted to calcium carbonate in approximately 50 min when the $CO_2$ flow rate was 200 mL/min. However, a comparable conversion was only achieved after 80 min when the flow rate was 50 mL/min. Despite this, it was not always advantageous to increase $CO_2$ flow rate to obtain a higher reaction rate. Because the $CO_2$ flow rate should be considered both by the reaction time and the $CO_2$ sequestration efficiency. Fig. 3c showed the effect of $CO_2$ flow rate on the $CO_2$ sequestration efficiency of product. As the reaction progress, the $CO_2$ sequestration efficiency was decreased. The $CO_2$ sequestration efficiency was 38.83% after 10 min when the flow rate was 50 mL/min, while it can reach approximately 84% when the flow rate was 100 mL/min (Fig. 3c). And it needed less time to finish the reaction when the $CO_2$ flow rate was 100 mL/min compared to 50 mL/min. When the $CO_2$ flow rate was 200 mL/min, it needed the same time to finish the reaction compared to 100 mL/min, but it had lower $CO_2$ sequestration efficiency (Fig. 3c).

The effect of the liquid to solid ratio on the carbonation of desulfurization residue was evaluated by adjusting the ratio from the range of 3-8 mL/g (C1, B2 and C2). A period of approximately 60 min was required to complete each reaction and the pH value of the solution was not significantly affected by changing the liquid to solid ratio (Fig. 4a). However, Fig. 4b showed that the liquid to solid ratio affected the carbonation ratio, which fell from 98% for B2 and C2 to 90% when the liquid to solid ratio was 3 mL/g. This indicated that the carbonation reaction was incomplete because of the lack of ammonia. The conditions in B2 were chosen as the optimal liquid to solid ratio.

The effect of the reaction temperature on the carbonation of desulfurization residue was evaluated by considering the temperatures of 20, 30 and 40 °C (D1, B2 and D2). The influence of reaction temperature on the desulfurization residue carbonation was not as strong as that of concentration of ammonia and $CO_2$ flow rate. Fig. 5a showed the pH variation of the reaction solution over time and showed that reaction time decreased with an increase in the reaction temperature. For all three experiments carbonation ratios of over 95% were observed (Fig. 5b). Considering the tradeoff between reaction time and energy consumption for heating, 30°C (B2) was chosen as the optimal reaction temperature.

The above research has clearly demonstrated the feasibility of using desulfurization residue for $CO_2$ sequestration with industry-grade. By following the optimized process, the carbonation ratio ($\eta$) can reach 98%, and 1 t desulfurization residue was able to sequester 373 kg of $CO_2$, a value greater than the other solid wastes obtained previously (Table 3). And approximately 1 t of desulfurization residue can absorb 373 kg of $CO_2$, where the process required 3.9 t of water and 1 t of industrial ammonia. In the carbonation process, ammonia can be recycled by calcining intermediate ($(NH_4)_2SO_4$). and 1 t ammonium sulphate was able to prepare 177 kg of ammonia. 1 t desulfurization residue was able to produce 900 kg of ammonium sulphate, and it can recycle 160 kg of ammonia ($12). Combining with previous research[33], we preliminarily estimated that the total cost of the whole desulfurization residue carbonation process (including energy consumption, reagent recovery and the value of the recycled agent) may be around $92 (Table 4), much lower than that of previous methods[33,34].

The reaction products from the desulfurization residue carbonation experiments were examined using XRD and SEM. After the carbonation reaction, the product containing calcium carbonate with purity above 94% and the crystalline phase of the carbonated desulfurization residue was mainly calcite with some vaterite also present (Fig. 6a), indicating the successful carbonation of desulfurization residue at a low temperature and ambient pressure under the action of ammonia. Fig. 6b showed the morphology and microstructure of carbonation products in the desulfurization residue after reaction with industry-grade $CO_2$. The carbonated sample showed a large number of spherical and granular particles, and they were agglomeration together (Fig. 6b).

Desulfurization residue is mostly generated from power generation and sintering plants. The generation of desulfurization residue is accompanied by a large amount of carbon dioxide emissions, so we explored the experiments that the desulfurization residue carbonation for $CO_2$ sequestration with the simulated

desulfurized flue gas in the following study. The experimental conditions used for simulated desulfurized flue gas were exactly the same to those used for the industry-grade $CO_2$ gas (except for the injection rate), and they were listed in Table 2. The injection rates of the gas mixture were 300, 400 and 500 mL/min (E1, E2 and E3).

Carbonation conducted by using simulated desulfurized flue gas was found to be slower compared to that conducted by using industry-grade $CO_2$. This fact could be inferred from the lower decrease rate of the pH of the gas mixture (Fig. 7a) compared to that in the case of industry-grade $CO_2$ gas. This tendency was more easily observed in the carbonation ratio curve in Fig. 7b. It could be seen that the carbonation reaction in the case of the gas mixture was not significantly affected through changing the mixed gas flow rate by comparing E1, E2 and E3 (Fig. 7b). The carbonation ratio could reach 90% after the reaction was done for 150 min in the case of E1, E2 and E3. Fig. 8 showed the XRD and SEM results of the carbonation product with simulated desulfurized flue gas. The crystalline phase of the carbonation product was mainly calcite, there was also some vaterite (Fig. 8a), indicating the successful carbonation of desulfurization residue with simulated desulfurized flue gas. The morphology of the carbonation product was rectangular and spherical (Fig. 8c&d). The injection of simulated desulfurized flue gas did not change the crystal phase and morphology of the carbonation product (Fig. 6&8), but the particles became smaller. Some calcite with a purity exceeding 99% and good crystal morphology could be obtained in the reaction filtrate in the case that simulated desulfurized flue gas was injected (Fig. 8b&d). Therefore, desulfurized flue gas could be used directly in the desulfurized residue carbonation process without any need for a separate $CO_2$ capture process.

The aqueous carbonation of materials with low porosity, such as desulfurized residue, is an irreversible and heterogeneous gas-liquid-solid reaction. $CO_2$ dissolved in the water and reacted with $Ca(OH)_2$ in the desulfurized residue particles and $NH_4OH$. This activity occurs during the kinetically controlled stage or the diffusion-controlled stage. An analysis of the relationship between η and t was conducted to study the kinetics of the desulfurized residue carbonation, in which the reaction kinetic equation of spherical particles (Eq.7) and the Ginstling equation of spherical particles (Eq.8)[35] were adapted to describe the kinetically controlled stage and the diffusion-controlled stage, respectively.

$$(1-\eta)^{-2/3}-1=k_1t \quad (7)$$

$$1-2\eta/3-(1-\eta)^{2/3}=k_2t \quad (8)$$

Where η is the carbonation ratio of desulfurized residue (%), t is the instantaneous reaction time (min), $k_1$ is the rate constant during the kinetically controlled stage ($min^{-1}$), and $k_2$ is the rate constant during the diffusion-controlled stage ($min^{-1}$).

The relationships of $\ln[(1-\eta)^{-2/3}-1]$ versus lnt and $\ln[1-2\eta/3-(1-\eta)^{2/3}]$ versus lnt at different concentration of ammonia, $CO_2$ flow rate, liquid to solid ratio and temperatures were shown in Fig. 9&10. $Ln[(1-\eta)^{-2/3}-1]$ and lnt in Fig. 9 showed a definite linear dependence generally during the carbonation process. While, $\ln[1-2\eta/3-(1-\eta)^{2/3}]$ and lnt in Fig. 10 did not well conform to the linear relationship. So, the reaction kinetic equation was a successful fit for the kinetically controlled stage during the carbonation of desulfurized residue regardless of the change in concentration of ammonia, $CO_2$ flow rate, liquid to solid ratio and temperature. However, the irregular and uneven shape of the actual desulfurized residue particles caused the slopes of these curves to deviate from the theoretical value (1.0) in varying degrees[36]. The rate constant $k_1$ could be derived and was showed in Table 5. Most of the $k_1$ rate constants derived in this study were higher than those calculated by Sun et al. [37], demonstrating theoretically that the reaction rate of desulfurized residue carbonation was significantly faster than the carbonation showed by Sun et al.[37]. Concentration of ammonia and liquid to solid ratio were the most important process variables for the desulfurized residue carbonation and had a strong influence on the kinetically stage. $k_1$ increased more than 6 and 4 times, from 0.0335 $min^{-1}$ at 1 mol/L to 0.212 $min^{-1}$ at 4 mol/L, and from 0.0528 $min^{-1}$ at 3 mL/g to 0.224 $min^{-1}$ at 8 mL/g, respectively. The influence of either the $CO_2$ flow rate or temperature on the carbonation of desulfurized residue was not as notable as the influence of concentration of ammonia and liquid to solid ratio. The final carbonation ratio almost increased when the rate constant $k_1$ increased, indicating that process variables such as concentration of ammonia, $CO_2$ flow rate, liquid to solid ratio and temperature could influence the carbonation ratio of desulfurized residue through a direct and definite influence on the corresponding rate constant.

The activation energy, which was E=20.21 kJ/mol ($R^2$=0.94) for the kinetically controlled stage was determined through a linear fitting of the plot of lnk versus 1/T according to the Arrhenius empirical formula[38]. The activation energy determined in this study was slightly lower than those reported by Tian et al.[36], which was 21.29 kJ/mol and slightly higher than those reported by Sun et al. [37], which was 14.84 kJ $mol^{-1}$ for the kinetically controlled stage.

## 4. Conclusions

The carbonation of desulfurization residue was studied both by theoretical and experimental approaches to evaluate the feasibility of its use for $CO_2$ sequestration. The desulfurization residue carbonation reaction followed the kinetically controlled stage mechanism, which could be effectively modeled with the reaction kinetic equation. The activation energy was 20.21 kJ/mol for the kinetically controlled stage.

Ammonia concentration, $CO_2$ flow rate, liquid to solid ratio and temperature affected the carbonation ratio of desulfurization residue through their direct and definite influence on the rate constant. Ammonia concentration and liquid to solid ratio were the most important process variables influencing the desulfurization residue carbonation in terms of both the carbonation ratio and reaction rate. The influence of either $CO_2$ flow rate or temperature was not as notable as ammonia concentration and liquid to solid ratio.

The desulfurization residue displayed high carbonation reactivity, even at low temperature and atmospheric pressure, producing calcite and vaterite with spherical and granular morphology. Under the optimized conditions (3 mol/L ammonia solution, 100 mL/min $CO_2$ flow rate, 5:1 mL/g liquid to solid ratio and a reaction temperature of 30 °C), calcium carbonate with >94% purity could be produced within 60 min with a carbonation ratio of approximately 98% and a maximum $CO_2$ sequestration of 373 $kg_{CO2}/t_{residue}$. The simulated desulfurization fuel gas in the



 

carbonation reaction had a relatively minor effect on the carbonation ratio. However, it slowed the carbonation reaction and produced a carbonation product with a smaller average particle size, which included high purity (≥99%) white calcite. This technique has the advantage of a rapid $CO_2$ sequestration ratio, low costs, and a large potential for in-situ $CO_2$ sequestration in the electricity and steel industry. Therefore, more pilot experiments should be undertaken to provide a practical foundation for future applications.

## Acknowledgements

This work was supported by the National Science Fund for Distinguished Young Scholars (51225403), the State Key Laboratory of Powder Metallurgy, Central South University, the Hunan Provincial Co-Innovation Centre for Clean and Efficient Utilization of Strategic Metal Mineral Resources, and the Fundamental Research Funds for the Central Universities of Central South University (2014zzts062).

## Notes and references

1. C. Stewart and M.-A. Hessami, *Energ Convers Manage*, 2005, **46**, 403-420.
2. S. Liu and H. Yang, *Appl Clay Sci*, 2014, **101**, 277-281.
3. J. Jin, J. Ouyang and H. Yang, *Appl Clay Sci*, 2014, **99**, 246-253.
4. R. Bredesen, K. Jordal and O. Bolland, *Chem Eng Process*, 2004, **43**, 1129-1158.
5. M. Mikkelsen, M. Jørgensen and F. C. Krebs, *Energ Environ Sci*, 2010, **3**, 43-81.
6. R. Shukla, P. Ranjith, A. Haque and X. Choi, *Fuel*, 2010, **89**, 2651-2664.
7. P. Friedlingstein, R. M. Andrew, J. Rogelj, G. P. Peters, J. G. Canadell, R. Knutti, G. Luderer, M. R. Raupach, M. Schaeffer, D. P. van Vuuren and C. Le Quéré, *Nat Geosci*, 2014, **7**, 709-715.
8. P. Falkowski, R. J. Scholes, E. Boyle, J. Canadell, D. Canfield, J. Elser, N. Gruber, K. Hibbard, P. Högberg, S. Linder, F. T. Mackenzie, B. Moore, T. Pedersen, Y. Rosenthal, S. Seitzinger, V. Smetacek and W. Steffen, *Science*, 2000, **290**, 291-296.
9. A. Sanna, M. Uibu, G. Caramanna, R. Kuusik and M. M. Maroto-Valer, *Chem Soc Rev*, 2014, **43**, 8049-8080.
10. X. Li and H. Yang, *Crystengcomm*, 2014, **16**, 4501-4507.
11. H. E. King, O. Plümper and A. Putnis, *Environ Sci Technol*, 2010, **44**, 6503-6509.
12. A.-H. A. Park and L.-S. Fan, *Chem Eng Sci*, 2004, **59**, 5241-5247.
13. W. J. J. Huijgen, G.-J. Witkamp and R. N. J. Comans, *Chem Eng Sci*, 2006, **61**, 4242-4251.
14. I. Stasiulaitiene, V. Vajegaite, D. Martuzevicius, G. Denafas, S. Sliaupa, J. Fagerlund and R. Zevenhoven, *Environ Prog Sustain*, 2014, **33**, 512-518.
15. H. H. Khoo and R. B. H. Tan, *Environ Prog*, 2006, **25**, 208-217.
16. F. Mahaut, G. Gauthier, P. Gouze, L. Luquot, D. Salin and J. Martin, *Environ Prog Sustain*, 2014, **33**, 572-580.
17. W. Ding, L. Fu, J. Ouyang and H. Yang, *Phys Chem Miner*, 2014, **41**, 489-496.
18. W. J. J. Huijgen, R. N. J. Comans and G.-J. Witkamp, *Energ Convers Manage*, 2007, **48**, 1923-1935.
19. M. M. Maroto-Valer, D. J. Fauth, M. E. Kuchta, Y. Zhang and J. M. Andrésen, *Fuel Process Technol*, 2005, **86**, 1627-1645.
20. M. Fernández Bertos, S. J. Simons, C. D. Hills and P. J. Carey, *J Hazard Mater*, 2004, **112**, 193-205.
21. S. Teir, S. Eloneva, C.-J. Fogelholm and R. Zevenhoven, *Energy*, 2007, **32**, 528-539.
22. J. Yu and K. Wang, *Energ Fuel*, 2011, **25**, 5483-5492.
23. W. J. Huijgen, G. J. Witkamp and R. N. Comans, *Environ Sci Technol*, 2005, **39**, 9676-9682.
24. R. Baciocchi, A. Polettini, R. Pomi, V. Prigiobbe, V. N. Von Zedwitz and A. Steinfeld, *Energ Fuel*, 2006, **20**, 1933-1940.
25. G. P. Assima, F. Larachi, G. Beaudoin and J. Molson, *Ind Eng Chem Res*, 2000, **51**, 8726-8734.
26. J.-H. Wee, *Appl Energ*, 2013, **106**, 143-151.
27. A. Iizuka, M. Fujii, A. Yamasaki and Y. Yanagisawa, *Ind Eng Chem Res*, 2004, **43**, 7880-7887.
28. S. Eloneva, S. Teir, J. Salminen, C.-J. Fogelholm and R. Zevenhoven, *Energy*, 2008, **33**, 1461-1467.
29. L. Yan, Y. Huaifen, Z. Bo, W. Shujuan, Z. Yuqun, C. Changhe and X. Xuchang, *Ecol Environ Sci*, 2010, **19**, 1682-1685.
30. M. G. Lee, Y. N. Jang, K. W. Ryu, W. Kim and J. H. Bang, *Energy*, 2012, **47**, 370-377.
31. K. Song, Y.-N. Jang, W. Kim, M. G. Lee, D. Shin, J.-H. Bang, C. W. Jeon and S. C. Chae, *Chem Eng J*, 2012, **213**, 251-258.
32. K. Song, Y. N. Jang, W. Kim, M. G. Lee, D. Shin, J. H. Bang, C. W. Jeon and S. C. Chae, *Energy*, 2014, **65**, 527-532.
33. S. J. Gerdemann, W. K. O'Connor, D. C. Dahlin, L. R. Penner and H. Rush, *Environ Sci Technol*, 2007, **41**, 2587-2593.
34. K. E. Kelly, G. D. Silcox, A. F. Sarofim and D. W. Pershing, *Int J Greenh Gas Con*, 2011, **5**, 1587-1595.
35. J. H. Sharp, G. W. Brindley and B. N. Narahari Achar, *J Am Ceram Soc*, 1966, **49**, 379-382.
36. S. Tian, J. Jiang, X. Chen, F. Yan and K. Li, *Chemsuschem*, 2013, **6**, 2348-2355.
37. J. Sun, M. F. Bertos and S. J. R. Simons, *Energ Environ Sci*, 2008, **1**, 370-377.
38. A. K. Galwey and M. E. Brown, *Thermochim Acta*, 2002, **386**, 91-98.
39. M. Back, M. Kuehn, H. Stanjek and S. Peiffer, *Environ Sci Technol*, 2008, **42**, 4520-4526.
40. S. C. Tian, J. G. Jiang, K. M. Li, F. Yan and X. J. Chen, *Rsc Adv*, 2014, **4**, 6858-6862.
41. G. P. Assima, F. Larachi, J. Molson and G. Beaudoin, *Chem Eng J*, 2014, **245**, 56-64.
42. M. Uibu, R. Kuusik, L. Andreas and K. Kirsimäe, *Enrgy Proced*, 2011, **4**, 925-932.

**Table 1** Composition of the desulfurization residue (wt %)

| CaO | $SO_3$ | $SiO_2$ | $Fe_2O_3$ | $Al_2O_3$ | $H_2O$ | Others |
|---|---|---|---|---|---|---|
| 48.45 | 25.75 | 0.55 | 1.98 | 2.49 | 18.1 | 2.68 |

Note: The chemical elements in the desulfurization residue are in the form of oxides.

**Table 2** Conditions of desulfurization residue carbonation

| | Desulfurization residue (g) | Ammonia concentration (mol/L) | $CO_2$ flow rate (mL/min) | Liquid to solid ratio (mL/g) | Temperature (°C) | $CO_2$ purity (%) |
|---|---|---|---|---|---|---|
| A1 | 20 | 1 | 200 | 5 | 30 | 99.9 |
| A2 | 20 | 2 | 200 | 5 | 30 | 99.9 |
| A3 | 20 | 3 | 200 | 5 | 30 | 99.9 |
| A4 | 20 | 4 | 200 | 5 | 30 | 99.9 |
| B1 | 20 | 3 | 50 | 5 | 30 | 99.9 |
| B2 | 20 | 3 | 100 | 5 | 30 | 99.9 |
| C1 | 20 | 3 | 100 | 3 | 30 | 99.9 |
| C2 | 20 | 3 | 100 | 8 | 30 | 99.9 |
| D1 | 20 | 3 | 100 | 5 | 20 | 99.9 |
| D2 | 20 | 3 | 100 | 5 | 40 | 99.9 |
| E1 | 20 | 3 | 300 | 5 | 30 | 10 |
| E2 | 20 | 3 | 400 | 5 | 30 | 10 |
| E3 | 20 | 3 | 500 | 5 | 30 | 10 |

**Table 3** Comparisons of $CO_2$ sequestration by solid wastes carbonations

| Raw material | Process conditions | Results | References |
|---|---|---|---|
| Coal fly ash | 75 °C, 50 g/L, 0.3 MPa, 600 rpm, 4.5 h | 230 kg($CO_2$)/t | [39] |
| Steel slag | Pretreated from 200 °C to 900 °C, carbonation at 600°C for 5 min at atmospheric pressure | 113 kg($CO_2$)/t | [40] |
| Blast furnace slag | Acetic acid and sodium hydroxide were used as agents, carbonation at atmospheric pressure and 30 °C | 227 kg($CO_2$)/t | [28] |
| Desulfurization gypsum | $NH_4OH$ was used as agent, carbonation at room temperature and atmospheric pressure | 243 kg($CO_2$)/t | [30] |
| Mining residues | Carbonation at room temperature and atmospheric pressure | 1.2-3.7 kg($CO_2$)/t | [41] |
| Oil shale ash | Carbonation at room temperature and atmospheric pressure | 90 kg($CO_2$)/t | [42] |
| Desulfurization residue | $NH_4OH$ was used as agent, carbonation at room temperature and atmospheric pressure | 373 kg($CO_2$)/t | This work |

**Table 4** Cost of raw material and treatment energy consumption of the proposed method

| Feed material | Costs ($/ton) | Treatment methodology | Treatment energy consumption kW·h/ton | Total costs ($) |
|---|---|---|---|---|
| Desulfurization residue | 20 | Grinding | - | 92 |
| Water | 0.735 | stiring (400 rpm) | 8 | |
| $NH_4OH$ | 75 | heat treatmenting | - | |
| | | filtering | 3 | |
| Ammonium sulphate | | Calcination | 50 | |

**Table 5** Rate constants for desulfurization residue carbonation calculated from model fitting

| Process variables | | $k_1/10^{-2}$ $min^{-1}$ | $R^2$ | Final η/% |
|---|---|---|---|---|
| Ammonia concentration (mol/L) | 1 | 3.35 | 0.944 | 75.5 |
| | 2 | 6.85 | 0.95 | 90.28 |
| | 3 | 21.1 | 0.959 | 97.62 |
| | 4 | 21.2 | 0.988 | 98.01 |
| $CO_2$ flow rate (mL/min) | 50 | 12.5 | 0.961 | 97.21 |
| | 100 | 24.2 | 0.976 | 98.01 |
| | 200 | 21.1 | 0.959 | 97.62 |
| Liquid to solid ratio (mL/g) | 3 | 5.28 | 0.958 | 90.58 |
| | 5 | 24.2 | 0.976 | 98.01 |
| | 8 | 22.4 | 0.978 | 98.21 |
| Temperature (°C) | 20 | 16.5 | 0.981 | 97.94 |
| | 30 | 24.2 | 0.976 | 98.01 |
| | 40 | 27.8 | 0.983 | 97.81 |

Journal Name RSCPublishing

PAPER

## Figures captions:

**Fig. 1.** (a) SEM image of the desulfurization residue, (b) EDS image of the desulfurization residue, (c) XRD pattern of the desulfurization residue, and (d) particle size distribution of the desulfurization residue.

**Fig. 2.** Effect of ammonia concentration on the desulfurization residue carbonation sample (a) pH of solution, (b) carbonation ratio of product.

**Fig. 3.** Effect of $CO_2$ flow rate on the desulfurization residue carbonation sample (a) pH of solution, (b) carbonation ratio of product, and (c) $CO_2$ sequestration efficiency of product.

**Fig. 4.** Effects of liquid-to-solid ratio on the desulfurization residue carbonation sample: (a) pH value of solution, (b) carbonation ratio of product.

**Fig. 5.** Effects of reaction temperature on the desulfurization residue carbonation sample (a) pH value of solution, (b) carbonation ratio of product.

**Fig. 6.** (a) XRD pattern of the desulfurization residue carbonation product and (b) SEM image of the desulfurization residue carbonation product with industry-grade $CO_2$ under optimum conditions (3 mol/L, 100mL/min, 5:1 mL/g and 30°C).

**Fig. 7.** Effects of $CO_2$-$N_2$-$O_2$ mixed gas on the desulfurization residue carbonation sample (a) pH value of solution, (b) carbonation ratio of product.

**Fig. 8.** XRD patterns of (a) the carbonation product with $CO_2$-$N_2$-$O_2$ mixed gas, (b) the carbonation product with $CO_2$-$N_2$-$O_2$ mixed gas in the filtrate, and SEM images of (c) the carbonation product with $CO_2$-$N_2$-$O_2$ mixed gas and (d) the carbonation product with $CO_2$-$N_2$-$O_2$ mixed gas in the filtrate under the conditions (3 mol/L, 300mL/min, 5:1 mL/g and 30°C).

**Fig. 9**. Plot of $\ln[(1-\eta)^{-2/3}-1]$ versus lnt for fitting the kinetically controlled stage at different process variables: (a) at different ammonia concentration (1, 2, 3, 4 mol/L), (b) at different $CO_2$ flow rate (50, 100, 200 mL/min), (c) at different liquid to solid ratio (3, 5, 8 mL/g) and (d) at different temperature (20, 30, 40 °C), $R^2$ is the linear correlation coefficient.

**Fig. 10**. Plot of $\ln[1-2\eta/3-(1-\eta)^{2/3}]$ versus lnt for fitting the diffusion-controlled stage at different process variables: (a) at different ammonia concentration (1, 2, 3, 4 mol/L), (b) at different $CO_2$ flow rate (50, 100, 200 mL/min), (c) at different liquid to solid ratio (3, 5, 8 mL/g) and (d) at different temperature (20, 30, 40 °C), $R^2$ is the linear correlation coefficient.

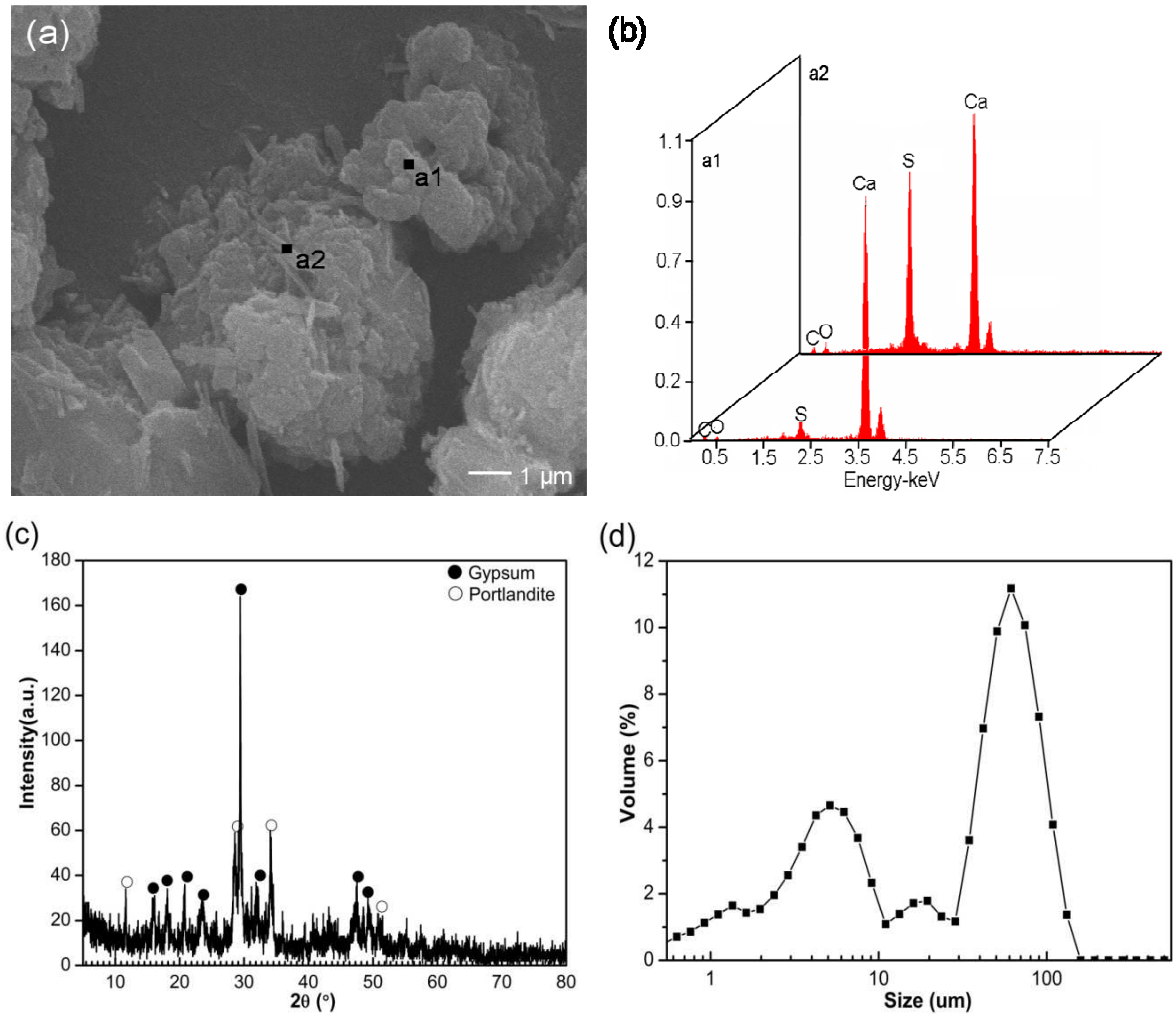


**Fig. 1** (a) SEM image of the desulfurization residue, (b) EDS image of the desulfurization residue, (c) XRD pattern of the desulfurization residue, and (d) particle size distribution of the desulfurization residue.

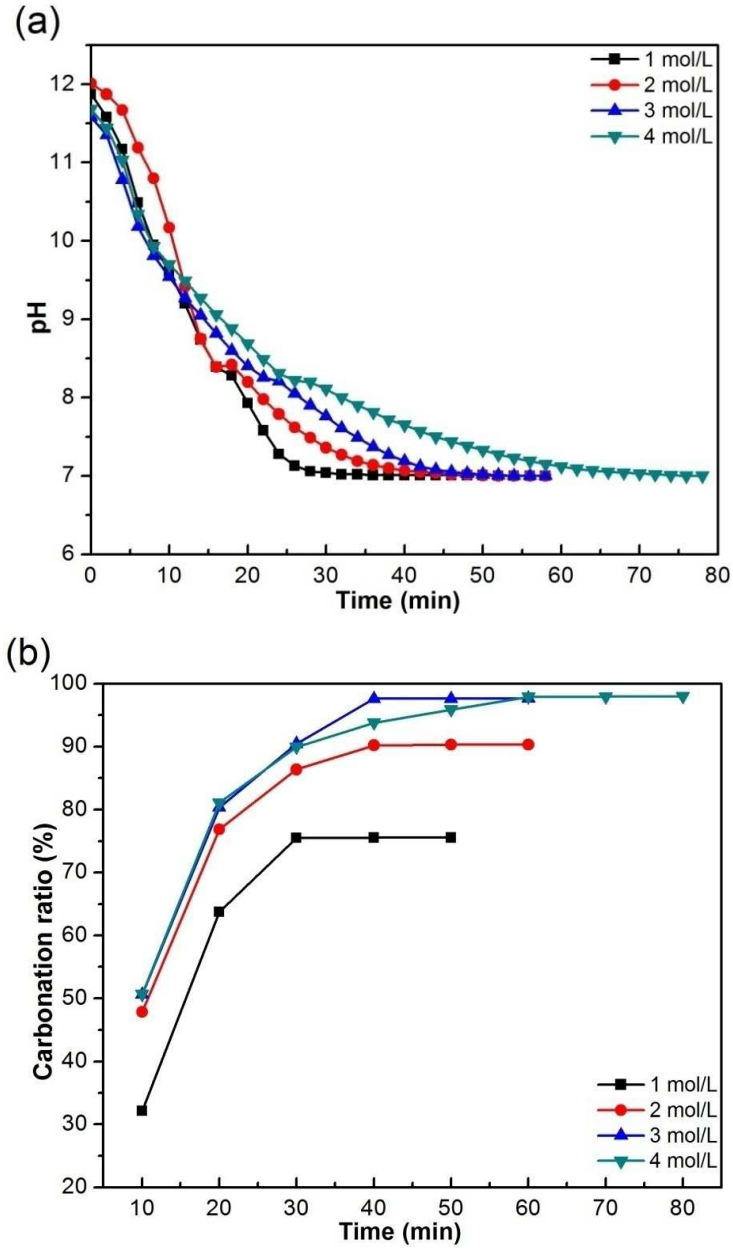


**Fig. 2** Effect of ammonia concentration on the desulfurization residue carbonation sample (a) pH of solution, (b) carbonation ratio of product.

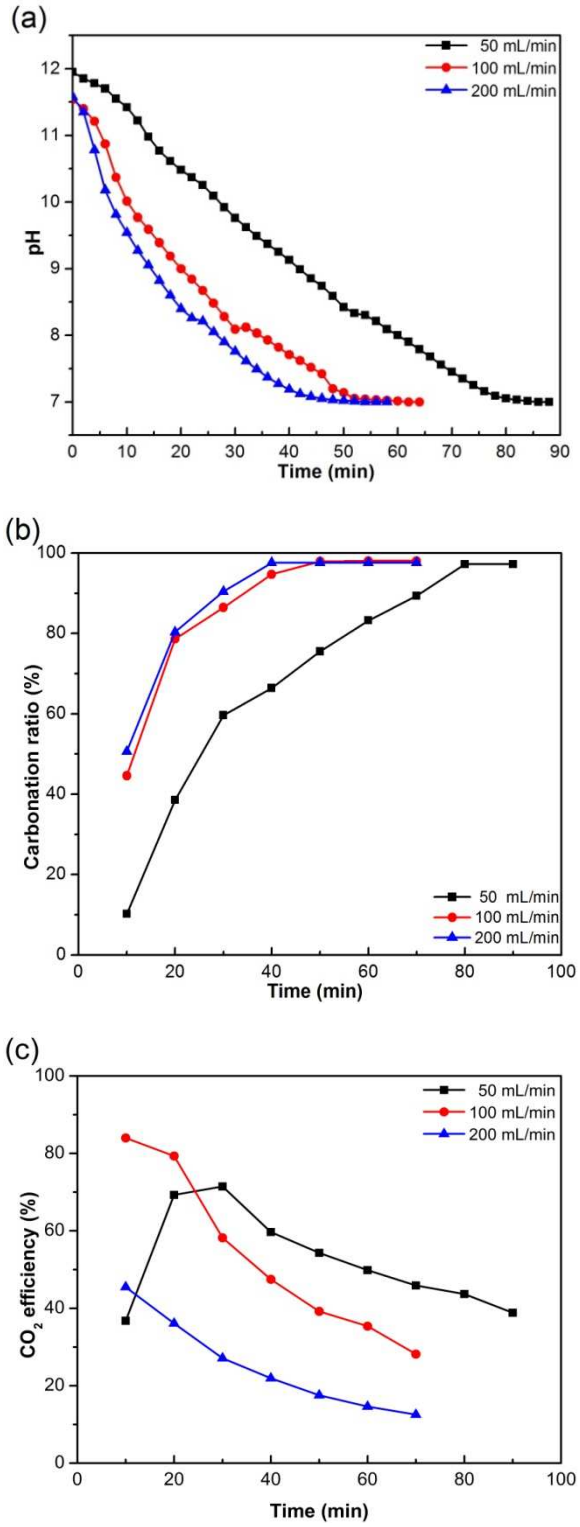


**Fig. 3** Effect of $CO_2$ flow rate on the desulfurization residue carbonation sample (a) pH of solution, (b) carbonation ratio of product, and (c) $CO_2$ sequestration efficiency of product.

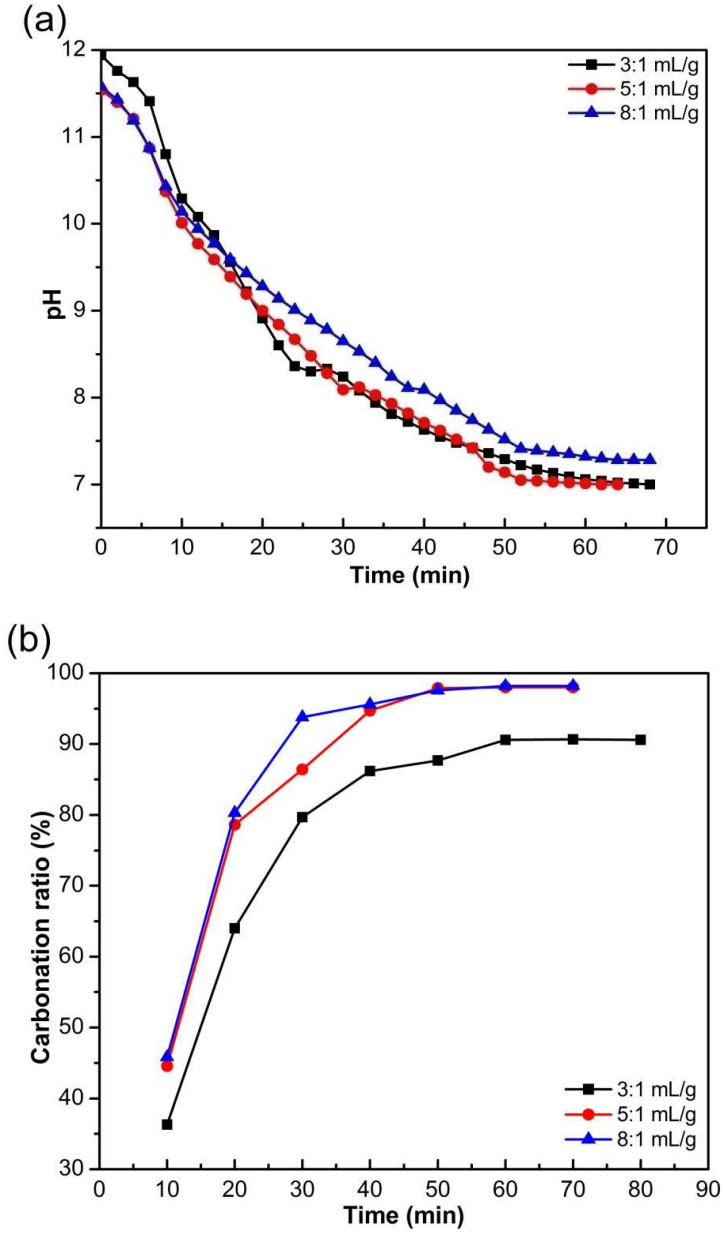


**Fig. 4** Effects of liquid-to-solid ratio on the desulfurization residue carbonation sample: (a) pH value of solution, (b) carbonation ratio of product.

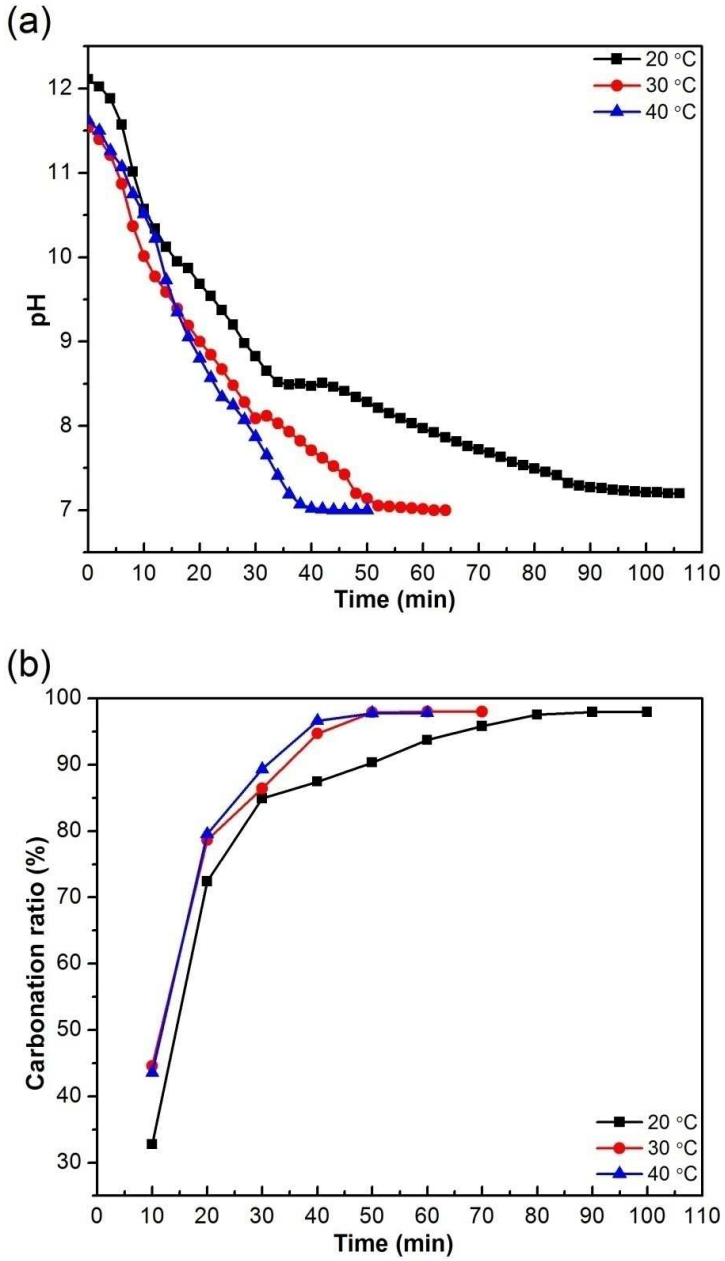


**Fig. 5** Effects of reaction temperature on the desulfurization residue carbonation sample (a) pH value of solution, (b) carbonation ratio of product.

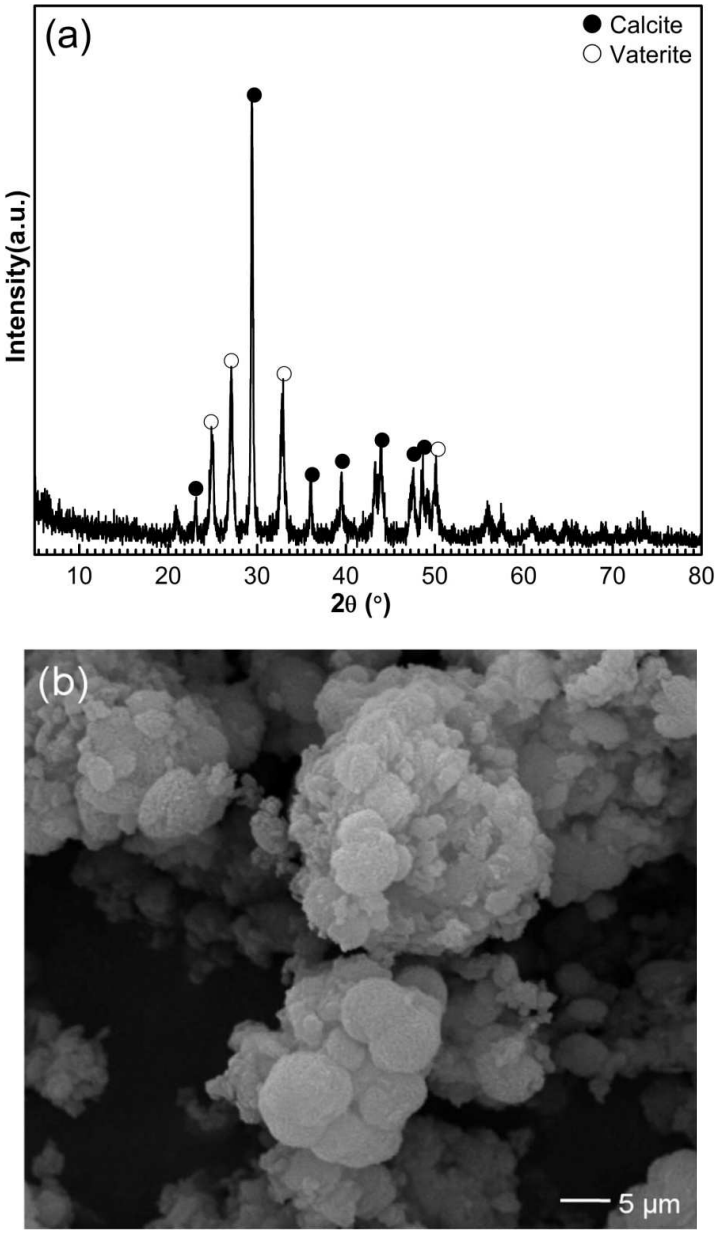


**Fig. 6** (a) XRD pattern of the desulfurization residue carbonation product and (b) SEM image of the desulfurization residue carbonation product with industry-grade $CO_2$ under optimum conditions (3 mol/L, 100 mL/min, 5:1 mL/g and 30°C).

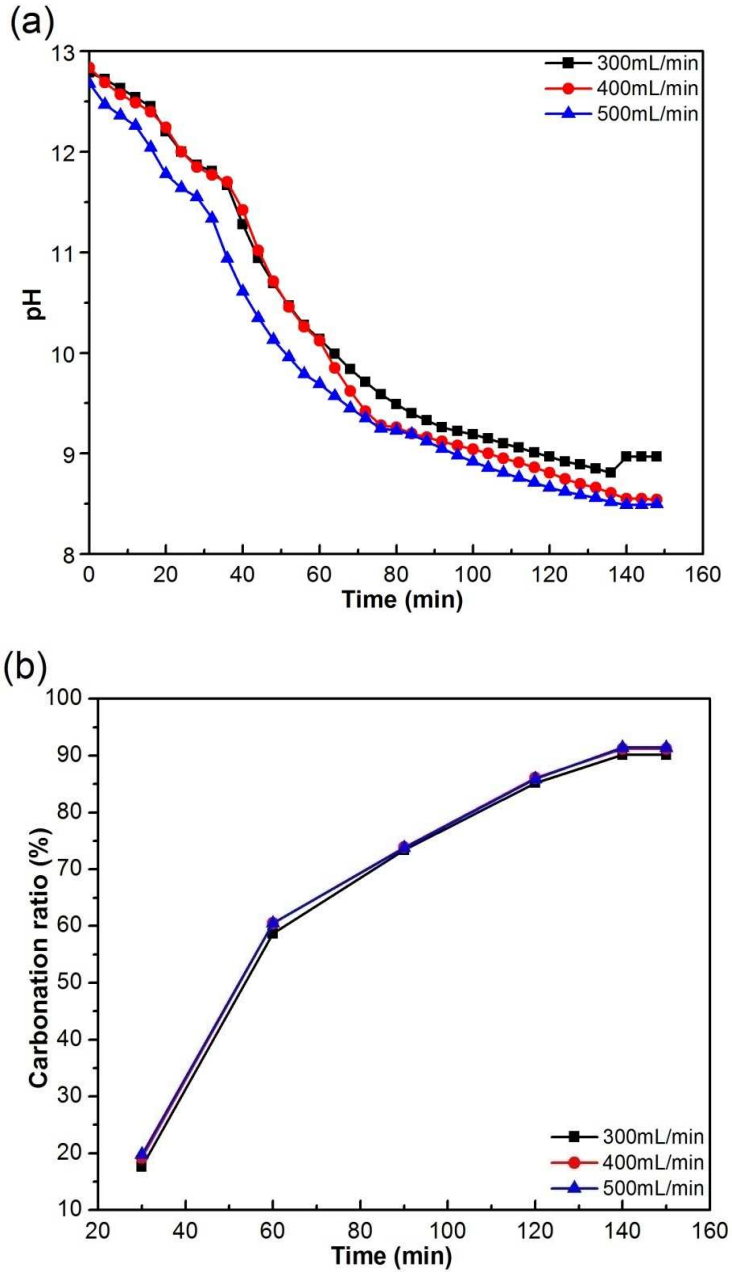


**Fig. 7** Effects of $CO_2$-$N_2$-$O_2$ mixed gas on the desulfurization residue carbonation sample (a) pH value of solution, (b) carbonation ratio of product.

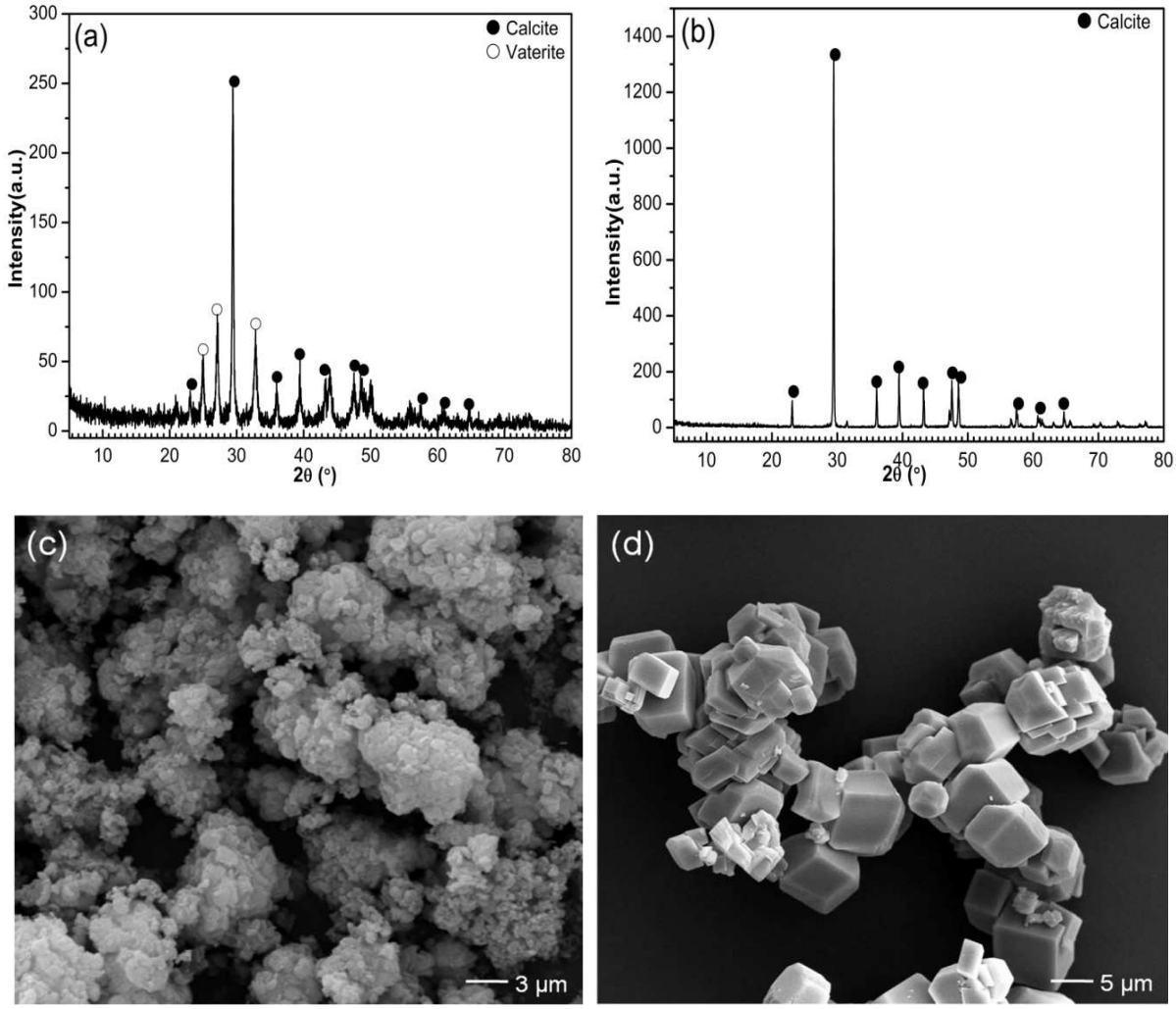


**Fig. 8** XRD patterns of (a) the carbonation product with $CO_2$-$N_2$-$O_2$ mixed gas, (b) the carbonation product with $CO_2$-$N_2$-$O_2$ mixed gas in the filtrate, and SEM images of (c) the carbonation product with $CO_2$-$N_2$-$O_2$ mixed gas and (d) the carbonation product with $CO_2$-$N_2$-$O_2$ mixed gas in the filtrate under the conditions (3 mol/L, 300 mL/min, 5:1 mL/g and 30°C).

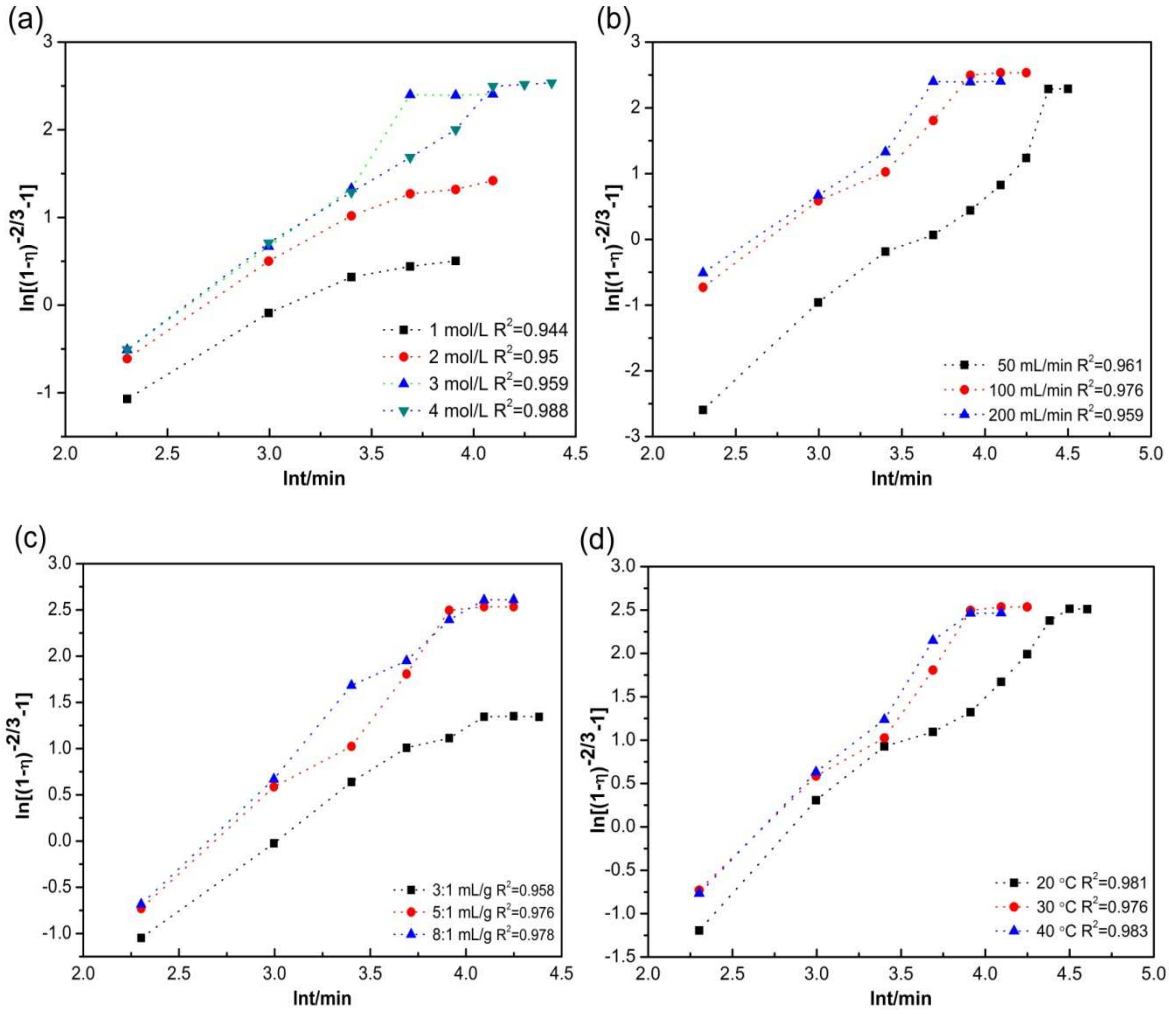


**Fig. 9**. Plot of $\ln[(1-\eta)^{-2/3}-1]$ versus lnt for fitting the kinetically controlled stage at different process variables: (a) at different ammonia concentration (1, 2, 3, 4 mol/L), (b) at different $CO_2$ flow rate (50, 100, 200 mL/min), (c) at different liquid to solid ratio (3, 5, 8 mL/g) and (d) at different temperature (20, 30, 40 °C), $R^2$ is linear correlation coefficient.

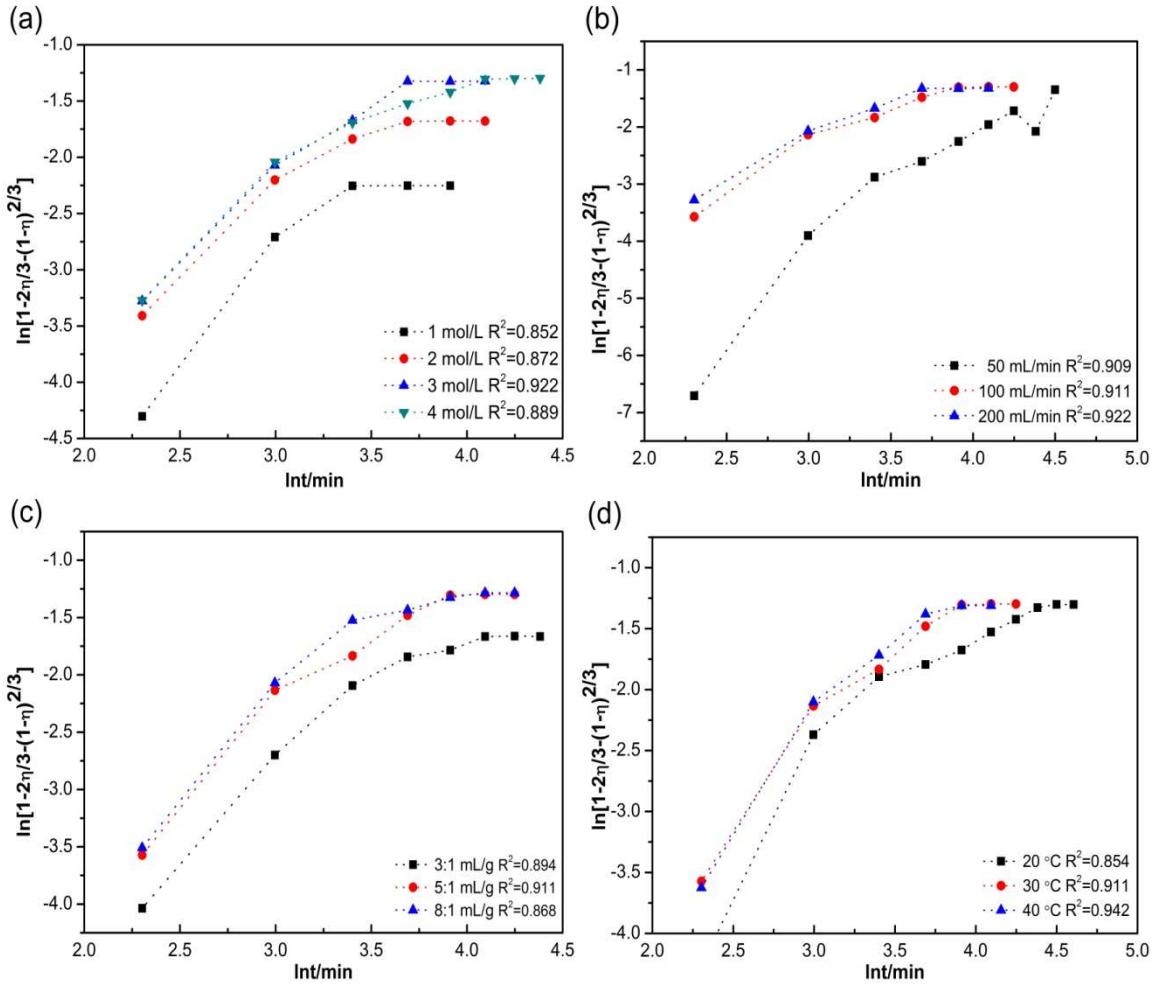


**Fig. 10**. Plot of $\ln[1-2\eta/3-(1-\eta)^{2/3}]$ versus lnt for fitting the diffusion-controlled stage at different process variables: (a) at different ammonia concentration (1, 2, 3, 4 mol/L), (b) at different $CO_2$ flow rate (50, 100, 200 mL/min), (c) at different liquid to solid ratio (3, 5, 8 mL/g) and (d) at different temperature (20, 30, 40 °C), $R^2$ is the linear correlation coefficient.